Theta and alpha oscillations are traveling waves in the human neocortex

Honghui Zhang,[1] Andrew J. Watrous,[1] Ansh Patel[1], & Joshua Jacobs[1]

[1] School of Biomedical Engineering, Columbia University, New York, NY 10027

Address correspondence to:

Dr. Joshua Jacobs
Department of Biomedical Engineering
Columbia University
351 Engineering Terrace, Mail Code 8904
1210 Amsterdam Avenue
New York, NY 10027
Phone: 212-854-2445
E-mail: joshua.jacobs@columbia.edu

Abstract

Human cognition requires the coordination of neural activity across widespread brain networks. Here we describe a new mechanism for large-scale coordination in the human brain: traveling waves of theta and alpha oscillations. Examining direct brain recordings from neurosurgical patients performing a memory task, we found that contiguous clusters of cortex in individual patients showed oscillations at specific frequencies in the range of 2 to 15 Hz. These clusters displayed spatial phase gradients, indicating that individual oscillation cycles moved across the cortex at ~0.25–0.75 m/s. We found that traveling waves were relevant behaviorally because their propagation correlated with task events and was more consistent during good performance. Traveling waves showed a correlation between propagation speed and temporal frequency, which suggests that they propagate across the cortex following principles of phase-coupled oscillatory networks. By demonstrating that theta and alpha traveling waves are widespread and behaviorally relevant, our results suggest a broad role for brain oscillations in supporting cortical connectivity by organizing neural activity across space and time.

Introduction

Oscillations have a distinctive role in brain function because they coordinate neuronal activity on multiple scales. Oscillations are important at the microscale, because they modulate the timing of neuronal spiking[1,2], and at the macroscale, where they synchronize distributed cortical networks that are communicating[3]. Owing to oscillations' ability to coordinate diverse neural processes, characterizing their spatiotemporal properties may reveal how neurons across multiple regions are dynamically coordinated to support behavior[4].

The human cortex displays oscillations at various frequencies during cognition[5]. To understand how these patterns relate to behavior, researchers have generally examined the properties of oscillations at individual frequencies in local networks[2,6] or in point-to-point links between distinct regions[7]. These approaches ignore a key feature of cortical oscillations that emerged from animal studies—that oscillations at multiple frequencies form spatially continuous neural patterns[8–10].

One such pattern is a traveling wave, which consists of a spatially coherent oscillation that moves progressively across the cortex, appearing like a wave moving across water. Cortical traveling waves have been studied most extensively in animal models, where they are observed most often in fine-scale recordings and were shown to be functionally important to various behaviors, including visual perception[11], spatial navigation[10,12], and movement[13]. In conjunction with predictions of computational models, these studies suggest that traveling waves are a key mechanism for guiding the spatial propagation of neural activity and computational processes across the brain[14].

Given the potential importance of spatially coordinated brain oscillations for large-scale cortical processes, several studies tested for large-scale synchronized oscillations—a prerequisite for traveling waves—in the human cortex. However, in humans such synchrony was rare or present only on a small scale[6,15,16]. These results shed doubt on the possibility that spatially coordinated patterns of oscillations such as traveling waves figured prominently in large-scale cortical processing in humans.

We re-examined the potential role of cortical traveling waves in human cognition by analyzing electrocorticographic brain (ECoG) recordings from seventy-seven neurosurgical patients (Table S1). We analyzed the data with a general technique that identifies traveling waves at the single-trial level across various frequencies and electrode configurations. As we describe below, we found alpha and theta traveling waves in 96% of subjects. Traveling waves were present across a wide frequency range (2 to 15 Hz), and were relevant behaviorally, as their propagation correlated with events and subject performance in a memory task. Our results suggest that human behavior is supported by spatial patterns of neuronal activity across the cortex that are carried by theta and alpha traveling waves.

Results

To identify traveling waves in the human cortex, we examined direct electrocorticographic (ECoG) brain recordings from neurosurgical patients performing a working-memory task[17]. This task has been shown previously to elicit large-amplitude oscillations related to memory at various frequencies[18–20]. Here, we analyzed these data using a new analytical framework that can identify synchrony and traveling waves by characterizing the spatiotemporal structure of the oscillations in each patient individually.

Spatial frequency clustering of oscillations. A traveling wave in the cortex of one patient would appear in ECoG signals as a neuronal oscillation that is visible simultaneously on multiple electrodes at the same frequency with a systematic timing (or phase) gradient across space, such that the oscillation appears to be propagating across space[14]. Thus, a first requirement for neural oscillations across multiple electrodes to display a traveling wave is that the signals must exhibit oscillations at the same frequency. Our first step in identifying human cortical traveling waves was to identify clusters of cortex where multiple neighboring electrodes recorded oscillations at the same frequency. To identify these patterns we examined the recording from each electrode individually and measured the frequencies of any narrowband oscillations that were present in the power spectrum. We identified these narrowband oscillations by using a peak-picking algorithm, which distinguished the narrowband oscillatory peaks that were elevated over the background $1/f$ ECoG power spectrum[21].

Using this technique, we identified electrodes with narrowband oscillations at various frequencies (Fig. S1A–D). In most patients there were spatially contiguous clusters of electrodes with narrowband oscillations at the same frequency (Fig. S1E–G). We refer to a contiguous group of four or more electrodes with oscillations at the same frequency as an *oscillation cluster* (see *Methods*). Across the dataset, we found 208 oscillation clusters across a total of 77 patients. Oscillation clusters were present at frequencies varying from 2 to 15 Hz, involved 58% of all electrodes, and were present in 96% of patients.

The frequencies of oscillation clusters often differed across individuals even for electrodes in the same anatomical region (Fig. S2). This suggested to us that oscillation clusters reflected distinctive cortical networks that were individualized for a given patient. To assess whether there were true intersubject differences in the frequencies of oscillation clusters, we tested for a spatial autocorrelation in the frequency of oscillations across the electrodes in each subject using Moran's I statistic[22]. This analysis tested the hypothesis that the frequencies of oscillations were more correlated between neighboring electrodes in a patient compared to electrodes at similar anatomical locations in other patients. We thus computed I for each subject and compared the results with those from a shuffling procedure that randomly interchanged electrodes between subjects. The mean with-subject frequency correlations ($I = 0.03$) were higher in the real data than in the shuffled data ($p < 10^{-3}$; Fig. S1G). This result indicated that clusters of electrodes with narrowband oscillations at the same frequency reflected robust within-subject spatial frequency clustering.

The widespread presence of oscillation clusters indicates that neuronal oscillations at a single frequency were present across large regions of the human cortex. If the timing of these oscillations were synchronized, it could provide evidence for large-scale oscillatory networks[4]. Thus, we next characterized the timing of activity across each oscillation clusters to identify patterns of phase synchrony such as traveling waves[13,20,23–26].

Human cortical traveling waves. Visual inspection of the signals from many oscillation clusters indicated that their phases were synchronized and that they indeed contained traveling waves. As one example, Figure 1A–C shows the activity across an 8-Hz oscillation cluster in an electrode grid from Patient 1. While 8-Hz oscillations were visible on all channels in this grid, the relative timing of this signal varied systematically with electrode location, such that the onset time of each oscillation correlated with the electrode's anterior–posterior position.

We quantified this phenomenon by calculating the relative phase of the oscillation on each electrode and trial (Fig. 1B). On this trial, oscillations showed a progressive spatial phase shift of ~240°. In this scheme, positive phase shifts correspond to oscillators that are further advanced. Thus, because the phase was largest at posterior electrodes, it indicates that on this trial there was an anterior-to-posterior traveling wave (see *Supplemental Movie* S1).

We used circular statistics[27] to measure the presence and properties of human cortical traveling waves by identifying patterns of oscillatory phase that shift systematically across the cortex. For each oscillation cluster, at each timepoint we used a circular–linear model to characterize the relation between electrode position and oscillation phase (Fig. 1D). This procedure models each cluster's instantaneous phase distribution as a planar wave, finding the best fitting spatial phase gradient. The fitted phase gradient provides a quantitative estimate of the speed and direction of traveling wave propagation (Fig. S3). We compute the quality of fit for each traveling wave on an electrode cluster by computing the proportion of phase variation that is explained by the planar wave model, which we call the phase gradient directionality (PGD).

We assessed whether each oscillation cluster exhibited a reliable traveling wave by testing its PGD value with a permutation procedure (Fig. 1E). This analysis demonstrated that traveling waves on the cluster in Figure 1A–C were statistically reliable (mean $PGD = 0.35$, $p < 0.001$) and consistently moving in an anterior-to-posterior direction ($\bar{r} = 0.94$, Rayleigh $p < 0.001$; Fig. 1F). Figure 1G–I shows example traveling waves in other patients that were also robust statistically.

We applied this methodology across our dataset and found that 140 (67%) of all oscillation clusters had consistent traveling waves, thus showing both reliable planar waves at the single trial level and a reliable direction of propagation. Traveling waves involved 47% of all electrodes and were present in all lobes of the neocortex across both left and right hemispheres (Table S2). Thus, traveling waves are a broad phenomenon across the neocortex.

To examine regional differences in traveling waves, we compared the properties of oscillation clusters identified from different brain areas (Fig. 2A; *Supplemental Movie* S2). Traveling waves from electrodes in the frontal and temporal lobes generally propagated in a posterior-to-anterior

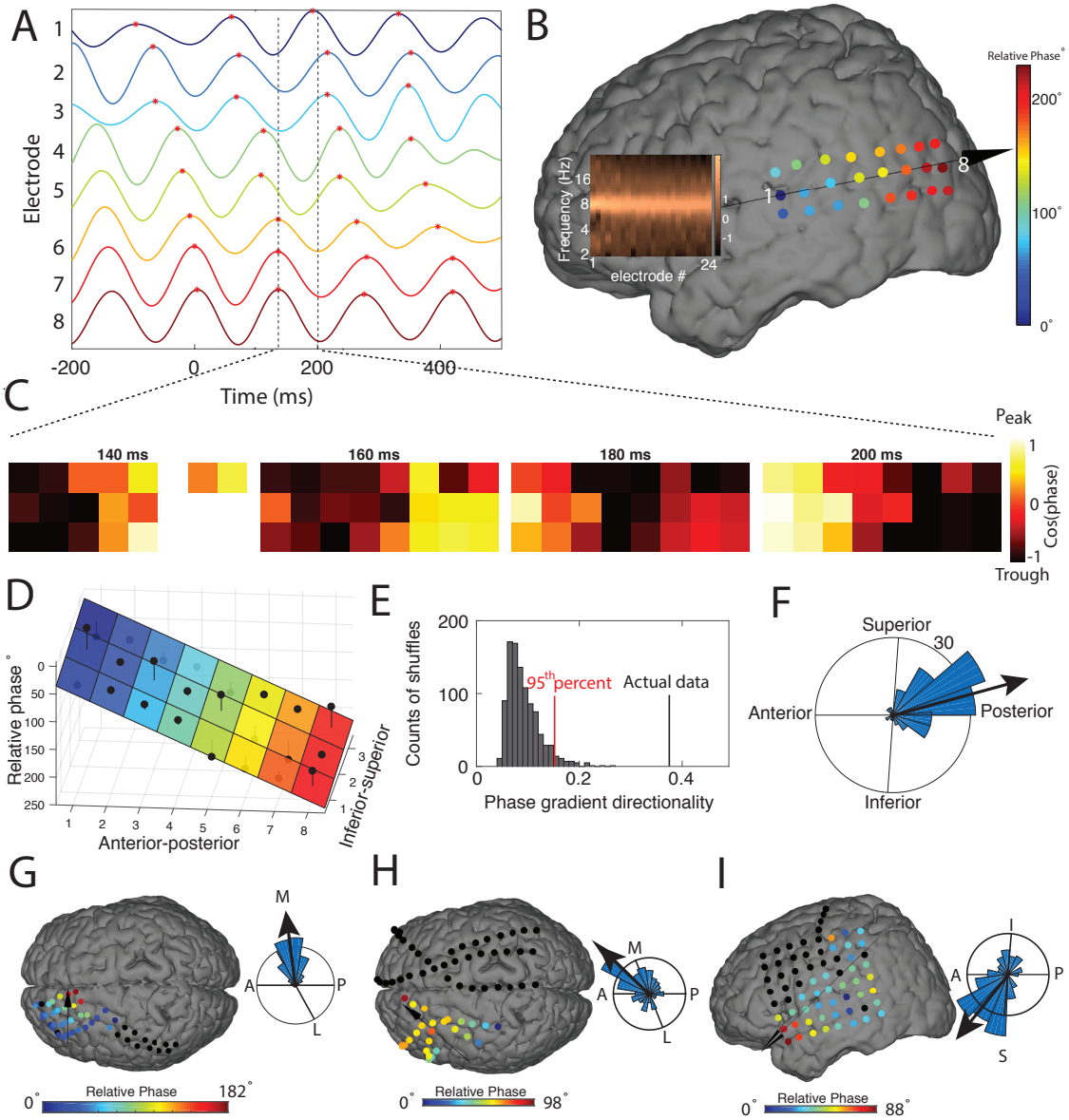

Figure 1: **Evidence for traveling waves in the human neocortex.** (A) An 8.3-Hz traveling wave in Patient 1. The plot shows this wave in one trial on electrodes ordered from anterior (top) to posterior (bottom). Peaks of individual oscillations are labeled with red asterisks, illustrating an increasing phase shift from anterior to posterior. (B) Relative phase of this traveling wave across the 3×8 electrode grid. Each electrode's color indicates the relative phase. Inset shows the normalized power spectrum for each electrode, demonstrating that all electrodes in the grid exhibit narrowband 8.3-Hz oscillations. Arrow indicates direction of wave propagation. (C) The temporal evolution of the phase pattern for the trial from Panels A & B. (D) Illustration of the fitted circular–linear model for quantifying spatial phase gradients and identifying traveling waves, applied to data from Panels A–C. Black dots indicate the average relative phase for each electrode; colored surface indicates the fitted phase plane; black lines indicate residuals. (E) Median phase gradient directionality (PGD) for this wave (black line). Gray bars indicate the distribution expected by chance. (F) Histogram indicating the directions of traveling-wave propagation observed on these electrodes across trials. (G–I) Phase distribution and direction for example traveling waves from Patients 3 (G), 63 (H), & 77 (I).

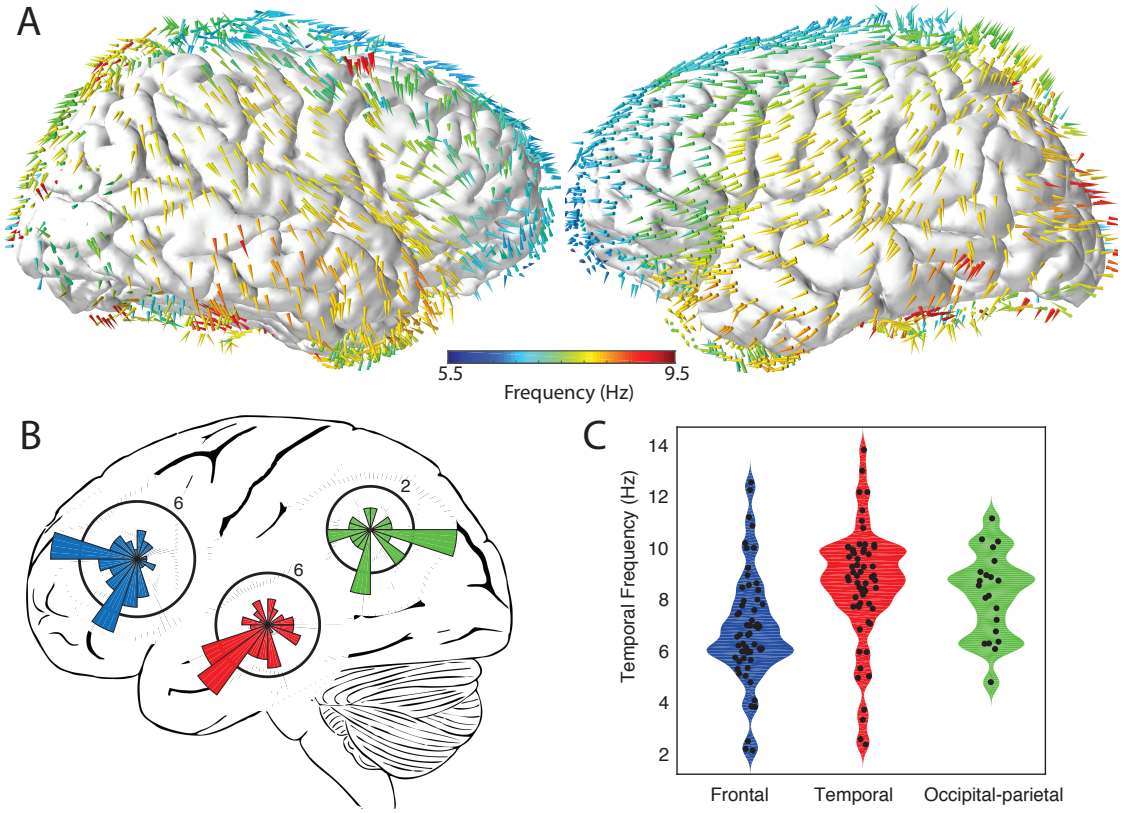

Figure 2: **Population analysis of traveling wave direction and frequency.** (A) Spatial topography of mean traveling-wave direction and frequency. Colored arrows indicate the mean direction and frequency of traveling waves observed at an electrode within 1.5 cm. (B) Distribution of the mean direction of traveling waves from each lobe. The orientations of the polar histograms are projected to match the lateral brain view. (C) Distributions of temporal frequencies for traveling waves from different regions. Black dots indicate the mean frequency from individual electrode clusters.

direction (p's< 0.01, Rayleigh tests; Fig. 2B). In the occipital and parietal lobes, traveling waves had a range of propagation directions that were not reliably clustered ($p > 0.05$). In the frontal lobe, traveling waves often propagated towards the midline.

We also compared the temporal frequencies of the oscillations that were involved in traveling waves (Fig. 2C). Individual traveling waves were present at frequencies ranging from 2 to 15 Hz. Traveling waves in the frontal lobe had slower mean temporal frequencies in the "theta" range (mean 6 Hz). In contrast, traveling waves in occipital and temporal regions had faster "alpha"-like frequencies (mean 9 Hz; ANOVA, $F_{(2,137)} = 9.7$, $p < 0.01$). It is notable that the frequencies of the traveling waves we found in frontal and occipital regions were similar to the theta and alpha oscillations that are commonly measured in these areas[28–30] because it suggests that these other oscillations are in fact traveling waves.

Behavioral relevance of cortical traveling waves. We hypothesized that the spatial propagation of traveling waves reflected the movement of neural activity across the cortex in a manner that was important for behavior. Although some previous studies had measured human cortical traveling waves during tasks, they did not show clear correlations to detailed features of behavior[26,31,32]. We tested for a potential functional role for traveling waves by measuring their dynamics through the course of memory processing. In each trial of this memory task[17], patients learned a list of stimuli and then viewed a retrieval cue. By comparing traveling-wave properties during this period, we hoped to identify functional properties of traveling waves and test if they differ across brain regions.

Figure 3A,B illustrates the timecourse of mean directional consistency (DC) during the cue response interval for the traveling waves on a cluster in the frontal lobe of from one patient. DC indicates the tendency for the traveling waves on a cluster to propagate in a single preferred direction. This plot indicates that the traveling waves on this cluster were not directionally organized at the moment of cue onset, but by 500 ms they reliably propagated in an anterior direction (DC=0.34). A different pattern was present for the traveling waves on an posterior electrode cluster in a different patient (Fig. 3C,D), whereby the directional organization was high at cue onset and subsequently decreased.

We quantified the dynamics of traveling wave DC at the group level, confirming that these patterns were reliable. During the course of the cue response interval, traveling waves on oscillation clusters in the temporal and frontal lobes showed increases in DC above baseline levels (Fig. 3E). Inversely, traveling waves from occipitoparietal clusters showed decreased DC during this same period. Thus, there are regional differences in the directional specificity of traveling waves from different regions (Fig. 3F; ANOVA, $F_{(2,137)} = 5.4$, $p < 0.01$)

We next examined whether traveling waves correlated with the efficiency of memory processing. We compared the DC of the traveling waves on each electrode cluster between trials where a patient had fast versus slow reaction times using a median split. Overall, DC positively correlated with performance, such that traveling waves moved more reliably in the preferred direction for each cluster on trials where the subject responded quickly to the retieval cue (Fig. 4). This effect was

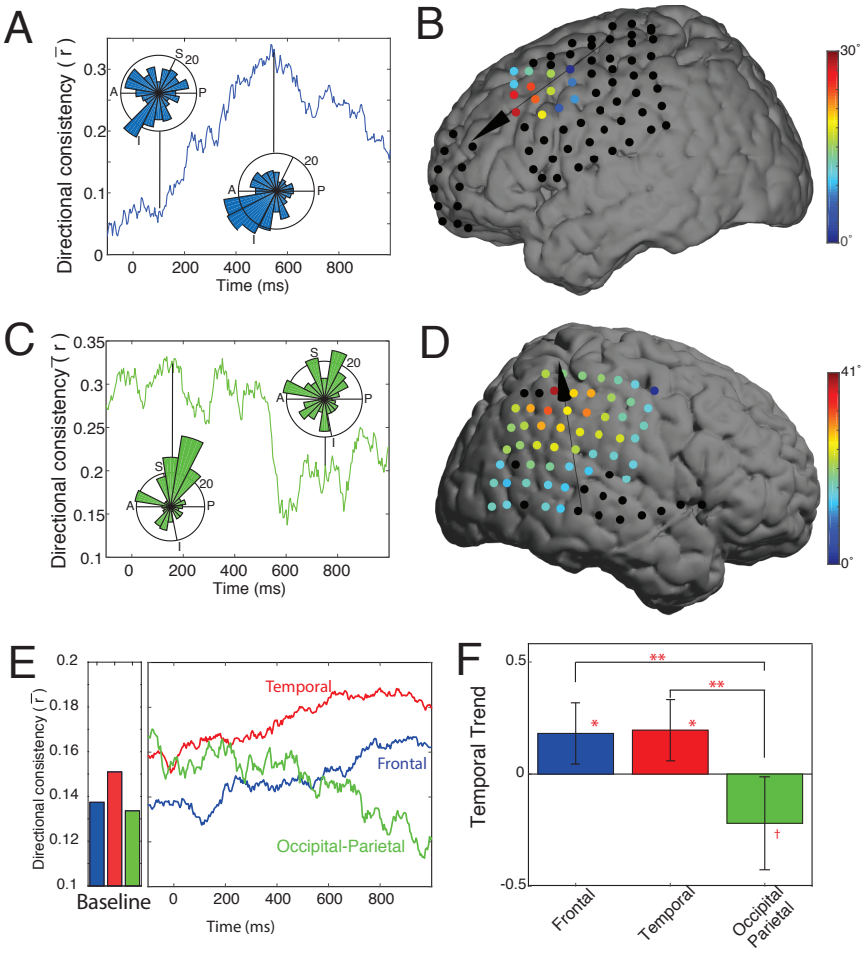

Figure 3: **Temporal dynamics of traveling waves.** (A) Timecourse of directional consistency (DC) for a traveling wave at 12.5 Hz from Patient 26's frontal lobe. Inset circular histograms indicate the distributions of propagation directions across trials at the labeled timepoints. (B) Brain plot showing the mean relative phase shift at each electrode at the timepoint of peak consistency (see Panel B). (C & D) Traveling 6.2-Hz parietoccipital wave from Patient 13, which showed a decrease in DC after cue onset. (E) Timecourse of traveling-wave DC. Bars indicate the mean DC for each region when patient is out of task (F) Analysis of DC slope. Positive values indicate that DC increases following cue onset. Error bars denote 95% confidence intervals. Post-hoc test: ** denotes $p < 0.01$; *, $p < 0.05$; †, $p < 0.1$.

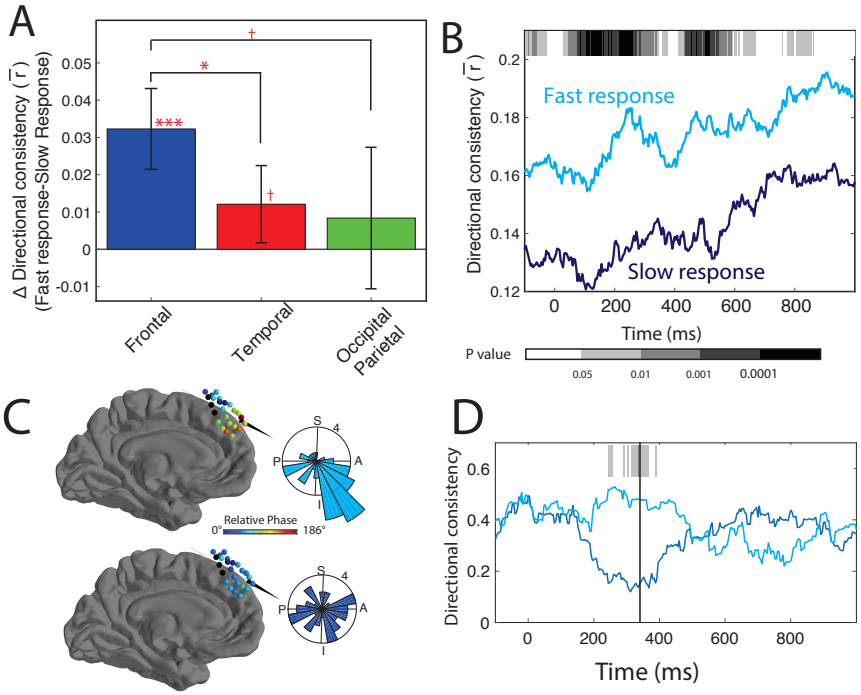

Figure 4: **Traveling waves and behavior.** (A) Mean difference in DC between fast and slow trials for 1 s after cue onset, separately calculated for each region. (B) Timecourse of mean DC in the frontal lobe between fast and slow trials. Gray shading indicates significance (paired t tests). (C) Time course of DC for data from Patient 3 that demonstrated elevated DC during trials where the patient responded rapidly. Shading indicates p values from a non-parametric circular direction distribution test[27] between fast and slow response trials. (D) Brain plot showing the mean relative phase distribution across an oscillation cluster in patient 3. Inset plot shows distribution of propagation directions across trials 220 ms after probe onset. (E) Same as D, for trials where the patient performed badly. Post-hoc test: $***$ denotes $p < 0.001$; $*$, $p < 0.05$; †, $p < 0.1$.

strongest for traveling waves in the frontal lobe ($F_{(2,137)} = 4.5$, $p = 0.013$), consistent with the notion that frontal theta oscillations are implicated in working memory[33,34].

We also examined how other properties of traveling waves varied in relation to memory efficency (Table S3). On trials where patients had fast reaction times there were increases in traveling wave PGD ($p = 0.003$) and in the power of the oscillations ($p < 0.001$). There were no reliable performance-related changes in traveling waves' temporal frequency, spatial frequency, or propagation speeds (all p's> 0.5). These results indicate that efficient neural processing is predicted by traveling waves maintaining their optimal propagation direction rather than waves moving at a faster speed or oscillating at a higher frequency.

Mechanisms of cortical wave propagation. To understand the physiological basis of human neocortical traveling waves, we compared their properties with the predicted characteristics from several theoretical models for this phenomenon[12,14]. Two theoretical models for traveling waves are the single-oscillator (SO) model and excitable-network (EN) models[14]. In the SO model, a traveling wave is produced when one oscillator projects to downstream areas via an array of gradually increasing conduction delays. In the EN model, traveling waves result from the gradual progression of excitatory activity across the cortex. Critically, the SO and EN models both predict that cortical traveling waves would move at a constant propagation speed, because the spatial propagation is a direct result of neuronal conduction delays, which are constant.

A third model of traveling waves is a network of weakly coupled oscillators (WCO)[12,14,20]. In the WCO model traveling waves are produced when there is a network of Kuramato oscillators[35] that show two properties: First, the oscillators must be arranged in a linear array, with with weak phase coupling between nearest neighbors. Second, there must be a spatial gradient in intrinsic frequency across the array of oscillators. When these two criteria are satisfied, oscillations will propagate in the direction of the frequency gradient, towards oscillators with slower intrinsic frequencies[36]. Critically, the WCO model predicts that oscillations with faster temporal frequencies propagate more rapidly because the traveling wave is a result of phase coupling[14,36].

We examined the propagation patterns of human traveling waves to distinguish the theoretical framework that best explained the physiological basis of this phenomenon. We measured the mean propagation speed for the traveling waves from each oscillation cluster (Fig. 5A & B). Traveling waves in individual patients varied substantially in mean propagation speed (mean=0.45 m/s, IQR 0.29–0.76). Furthermore, we found a positive correlation between propagation speed and oscillation frequency—waves with faster temporal frequencies propagated more rapidly. This frequency–speed correlation was present both at the group level, by comparing mean propagation speeds of waves from different electrode clusters ($r = 0.47$, $p < 10^{-7}$; Fig. 5C), and at the single-trial level, by measuring separate waves observed on different timepoints from the same electrodes (Fig. S4A). Critically, this positive correlation between a traveling wave's temporal frequency and propagation speed fits the predictions of the WCO model. In contrast, the SO and EN models predict that traveling waves propagate at a constant speed.

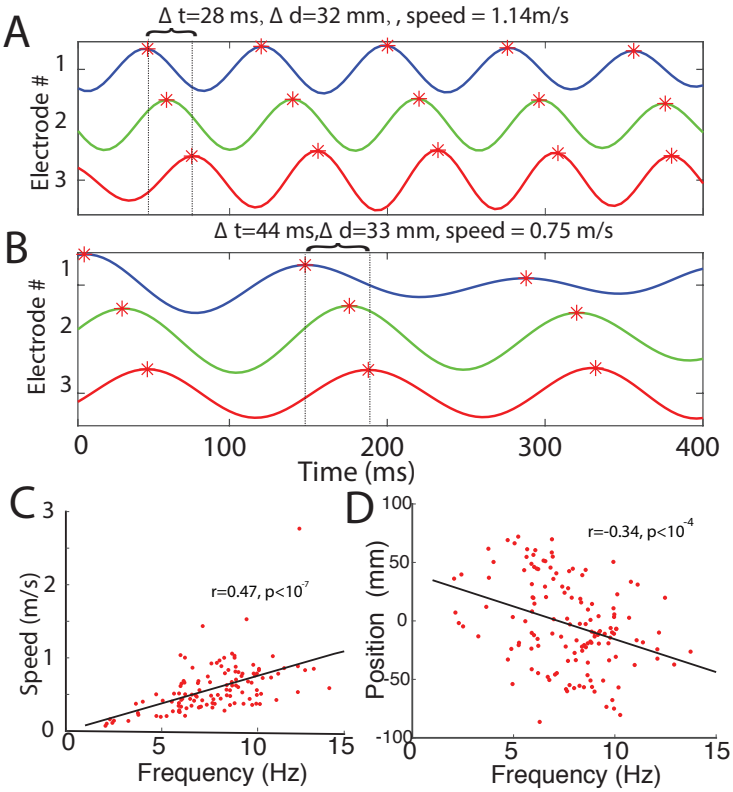

Figure 5: **Characteristics of traveling-wave propagation.** (A) Simultaneously recorded waveforms from three electrodes in a cluster with a 12.5-Hz traveling wave in Patient 26. This wave propagated at 1.14 m/s. Black dotted lines indicate the onset times of two oscillatory peaks. Labels indicate calculations used to measure this wave's propagation speed; Δt, delay between the arrival time of the oscillation between electrodes 1 & 3; Δd, distance in mm between electrodes 1 & 3, after correction for the angle of incidence of wave propagation. (B) Plot showing the measurement propagation speed for a 7.5-Hz traveling wave from Patient 39, which moved at 0.75 m/s on this trial. (C) Population analysis of the relation between traveling-wave propagation speed and frequency. Each point indicates the mean frequency and propagation speed of traveling waves from one oscillation cluster. Black line is a least-squares fit. (D) Population analysis of the relation between traveling-wave frequency and cluster location along the anterior–posterior axis (Talairach coordinates [mm]).

Furthermore, the WCO model also predicts the direction of wave propagation that we observed. In the WCO model, traveling waves propagate towards the oscillators with the slowest intrinsic frequencies[36]. This pattern was shown to exist in the rodent hippocampus[12,37]. The human cortical traveling waves that we observed also demonstrate a correlation between propagation direction and the frequency of the local oscillation. At the group level, there was a systematic decrease in oscillation frequency along the brain's posterior-to-anterior axis ($r = 0.34$, $p < 0.001$, Fig. 5D; Fig. 2A), which matches the mean propagation direction that also followed this same direction. This supports the idea that traveling waves generally propagate in a posterior-to-anterior direction because they are coordinated by an overall decrease in intrinsic oscillation frequency from posterior to anterior regions[29].

Although the majority of traveling waves propagated in a posterior-to-anterior direction, some exceptional oscillation clusters reliably showed traveling waves with the opposite propagation direction (e.g., Fig. 1). The WCO model predicts that the propagation direction for each traveling wave is determined by the orientation of the local oscillation frequency gradient. We thus compared the directions of frequency gradients and wave propagation at the individual cluster level to provide a more detailed test of the WCO model. Figures 6B & C shows the direction distribution for traveling-wave propagation and for frequency gradients at the single-trial level for the oscillation cluster in Patient 1. Notably, both of these distributions have means near zero, which suggests that these variables are related. We next examined the correspondence between the directions of wave propagation and frequency gradients at the group level. Here, for each oscillation cluster with a traveling wave, we computed the direction of the mean frequency gradient and the mean direction of wave propagation and then computed their difference. The pairwise direction differences were clustered near zero (Rayleigh test $p < 0.01$; Fig. 6D), which suggests that there was a positive correlation between the direction of frequency gradients and propagation directions for individual clusters.

In summary, the WCO model provides a good fit for our results because it illustrates how the direction and speed of the traveling waves we observed can be predicted by the local frequencies of the oscillations we measured. The WCO model suggests that the existence and direction of traveling waves are modulated by two factors: the strength of local phase coupling and spatial gradients of intrinsic oscillation frequencies[14,36]. When phase coupling is absent, there are no traveling waves because intrinsic oscillation frequencies differ between electrodes (Fig. 6E). When phase coupling is present, traveling waves emerge, propagating in the direction of decreasing oscillation frequency (Fig. 6F–G).

Discussion

Our findings demonstrate a new role for theta- and alpha-band neuronal oscillations by behaving as traveling waves, in addition to their known roles in supporting neuronal coding[38] and modulating synaptic plasticity[39]. Researchers had previously known that oscillations modulated cortical

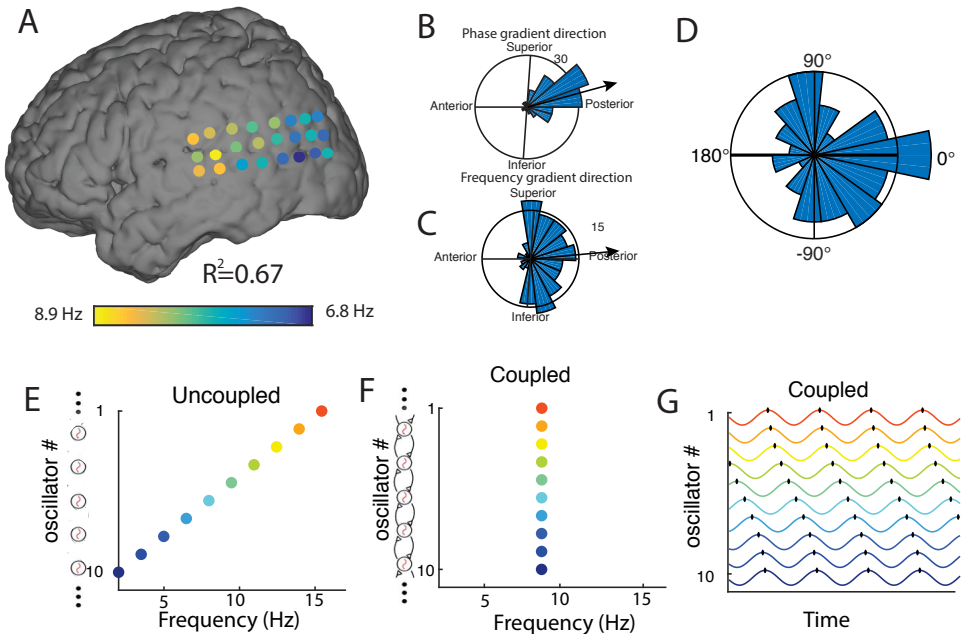

Figure 6: **Mechanisms of traveling waves.** (A) The instantaneous frequency distribution across electrodes of a traveling wave from same patient as Fig. 1 on one trial, demonstrating an anterior-to-posterior decreasing spatial-frequency gradient ($r^2 = 0.67$). (B) Distribution of the direction of traveling-wave phase propagation across all trials on this cluster (reproduced from Figure 1F). (C) Distribution of the direction of the spatial frequency gradients across these electrodes. In B & C, black lines indicate the mean gradient directions, thus demonstrating a correspondence between the directions of phase and frequency gradients. (D) Distribution of angular differences between each traveling-wave's mean phase gradient direction (propagation direction) and frequency gradient direction. The mean of the distribution is clustered near zero degree suggesting the propagation of each wave matches with their own frequency gradient ($p < 0.01$, rayleigh test). (E–G) Illustration of a model of weakly coupled oscillators[36] with parameters matched to our findings. Color indicates intrinsic frequency. When there is no phase coupling (Panel E), individual oscillators demonstrate their intrinsic oscillation frequencies from 2 Hz (anterior) to 16 Hz (posterior). When phase coupling is present (Panels F–G), all oscillators have the same temporal frequency (F) and a traveling wave emerges (G).

interactions in a point-to-point fashion between specific cortical areas[40,41]. Our results add to this work by demonstrating that oscillations also coordinate neural processing across large contiguous extents of human cortex. Neocortical traveling waves are prominent in the theta and alpha frequencies which, notably, also participate in the phenomenon of cross-frequency coupling (CFC)[42]. In CFC, the local oscillatory phase is coupled to the simultaneous amplitude of neuronal spiking[2] and to high-frequency oscillations[26,42]. If individual regions simultaneously exhibit both traveling waves as well as CFC[26], it indicates that bands of neuronal spiking activity propagate across the cortex during cognition. Based on the measurements of the traveling waves we observed, it suggests that these bands would have a median width of ~2.4–4.8 cm (Fig. S6) and a mean propagation speed of ~45 cm/s.

Studies of perception find that human sensory processing is supported by a sequence of discrete behavioral states. Scalp recordings indicated that individual states correspond to separate cycles of alpha oscillations[43]. Combined with our findings, these results suggests that individual traveling-wave cycles represent spatially discrete pulses of neural activity that correspond to distinct behavioral states. Therefore an engaging area of future work is to identify the degree to which traveling waves are relevant functionally for large-scale neural computation by providing a general mechanism for propagating discrete "packets" of neuronal activity across the cortex[44]. In this way, cortical traveling waves may provide a timing mechanism to distinguish distinct network states across space and time, in a similar fashion to theta oscillations in the hippocampus, where individual oscillation cycles temporally segment the representations of different cognitive maps[45]. Synchronized oscillations in multiple regions can form carrier signals that allow the representation of detailed behavioral information via phase and amplitude modulation[8,10]. It is thus possible that neocortical traveling waves also participate in the neural encoding of behavioral information via amplitude or phase modulation[44].

An issue for future investigation is understanding the functional relevance of each traveling wave's propagation direction. Most of the traveling waves we observed propagated in a posterior-to-anterior direction. Given the visual nature of the memory task that subjects performed, it seems reasonable to suspect that these waves followed the feedforward propagation of neural activity from low- to high-level visual areas[46]. In addition to visual regions, other brain areas also show posterior-to-anterior gradients in the abstractness of neural representations, such as the coding of spatial location in the hippocampus[12], the representation of task rules in the frontal lobe[47], and the nature of object representations in the temporal lobe[48]. It is notable that all these gradients tend to have a posterior-to-anterior orientation, matching the mean direction of traveling wave propagation. This suggests that traveling waves could be involved in the progressive transformation of neural representations in multiple cortical regions.

Although they were in the minority, some traveling waves showed the opposite pattern by propagating in an anterior-to-posterior direction. Understanding the relevance of this exceptional pattern remains an open question. One possibility is that the unusual traveling waves had a different functional role. In monkeys, visual alpha-band oscillations are linked to feedback processes[49],

which suggests they may propagate in an anterior-to-posterior direction. Likewise, it is possible that human anterior-to-posterior traveling waves could have a different functional role such as supporting feedback or top-down processes.

A notable feature of our results is that we found similar patterns of traveling waves in both the theta and alpha bands. Traditionally, human brain oscillations in the theta and alpha ranges have been linked to distinct processes—memory and idling, respectively[28]. By showing that both theta and alpha oscillations can be traveling waves and that they often propagate in the same direction, it suggests that these two oscillations are similar functionally and physiologically. The coupled oscillator model suggests that the specific frequency of a traveling wave depends on the intrinsic frequencies of the regions where it is propagating. Based on this idea, individual traveling waves could appear at different frequencies according to their destination. Thus, the specific "theta" or "alpha"frequency of a traveling wave could reflect regional differences in where the signal is propagating[7], rather than being the result of distinct physiological processes.

Some elements of the traveling waves we observed were noted in previous human studies[25,26,50]. A differentiating feature of our approach that allowed us to identify this signal more extensively was that we identified traveling waves across multiple brain regions and frequencies in individual subjects and trials. Because individual subjects exhibited traveling waves at different frequencies and directions in many regions, it suggests that there are true intersubject differences in the spatial and temporal structure of brain oscillations and traveling waves that are not possible to accurately capture with group-average analyses. Going forward it will be important to characterize the nature and potential functional relevance of these intersubject differences.

In addition to traveling waves, it is likely that the brain also exhibits other types of more-complex spatial patterns of oscillations, such as phase cones and spirals[51,52]. The brain may also exhibit spatial patterns of oscillations at faster frequencies or at finer spatial scales[13,44]. To characterize this rich set of dynamic spatial patterns, it may be useful to measure human cortical activity with electrodes that provide higher spatial resolution[53,54] rather than the 1-cm spaced electrodes we used. It may also be useful to utilize more sophisticated analysis methods that can characterize spatial patterns with a richer spatial structure rather than our methods that are limited to measuring planar waves.

Although our data came from epilepsy patients, it is unlikely that our results are driven by epileptiform brain signals. Epileptic activity does shows spatial propagation patterns[55], but this is was unlikely to be captured by our analysis methods. Our data analysis focused on theta- and alpha-band oscillations, which are known to be engaged by this type of working memory task[18]. Moreover, the theta and alpha oscillations that we observed here show task-related modulations that were consistent with noninvasive studies from healthy individuals[56]. Furthermore, noninvasive brain recordings from healthy individuals show spatial patterns that are entirely consistent with the traveling waves we observed[25].

Our work focused on assessing traveling waves in direct cortical recordings, but there is indeed evidence that similar patterns may be visible in noninvasive brain recordings[25]. The ability to

measure features of traveling waves at the group level may have significant practical implications. Researchers and clinicians examining noninvasive brain recordings should consider that aspects of their findings may result from spatially distributed oscillations such as traveling waves rather than precisely localizable point sources[57]. Whereas many electrical signals from the brain are commonly interpreted as event related potentials or as task-induced power changes of local oscillators; Instead, it is possible that many of these signals could result from the emergence of traveling waves that become transiently organized at a particular timepoint and phase across a cortical region. To distinguish the contributions of traveling waves to these signals, rather than the common analysis method of measuring the mean voltage or oscillatory power from each electrode individually[56], it may be useful to first identify traveling waves on a single-trial basis at each region and compare their timing and direction across trials, following our approach.

In addition to its benefits for research, the potential for non-invasively measuring traveling waves on a single-trial basis may have useful for the development of brain–computer interfaces. Furthermore, given the variations in traveling-wave properties that we observed across patients (Fig. 1), it seems important to characterize these patterns individually for each subject rather than only averaging across individuals. Then, having identified a reliable traveling wave pattern in an individual, there are many quantifiable properties of these signals that provide key insights into instantaneous neural processes, including speed, direction, coherence, frequency, spatial extent, and shape. Measuring traveling waves' instantaneous properties may provide a new tool for neural interfacing for tracking a subject's attention or cognitive state for timing stimulus presentation or modulating neuromodulation[58].

Methods

Subjects and Task. We examined direct brain recordings from 77 epilepsy patients who had electrodes surgically implanted to guide seizure mapping. Individual patients were implanted with a configuration of electrodes customized according to their clinical needs, which included both electrocorticographic (ECoG) surface grid and strips as well as depth electrodes. Our data collection was a continuation of previous reported study[19] and recordings were made at four hospitals (Thomas Jefferson University Hospital, Philadelphia; University of Pennsylvania Hospital Philadelphia; Children's Hospital of Philadelphia, and University Hospital Freiburg). All patients consented to having their brain recordings used for research purposes and the research was approved by relevant Institutional Review Boards. For the work described here, we examined only ECoG grid and strip electrodes on the cortical surface. The spacing between neighboring electrodes was 10 mm (center-to-center).

During free time between clinical procedures, these patients performed the Sternberg working memory task[17] on a laptop computer at their bedside. Each trial of the task consisted of two phases. In the first phase they memorize a short list of items. The second phase involves memory retrieval. Here they view a probe item and press a key to indicate if the probe was present in the remembered

list. Task performance was excellent, with patients having a mean accuracy of 90% and mean reaction time of 1.76 s. Our data analyses examined brain recordings during memory retrieval because it let us compare properties of patients' brain signals to their simultaneous behavioral performance[56].

Data acquisition. The electrical activity from each electrode was recorded by a clinical recording system whose timing was synchronized with the task computer. We pre-processed the data by downsampling the recordings to 250 Hz and performing an anatomically weighted average re-referencing[19]. We identified the location of each recording electrode by co-registering a pre-surgical structural magnetic resonance image (MRI) image with a post-operative computed tomography (CT) image. From these images, we identified the location of each recording contact on the CT images and computed the electrode location in standardized Talairach coordinates[59].

Identifying spatial clusters of electrodes with similar oscillations. Given our interest in characterizing propagating traveling waves, we designed an algorithm to identify spatial clusters of electrodes with narrowband oscillations at the same frequency. This algorithm accounted for several complexities of human brain oscillations measured with ECoG signals, including differences in electrode positions across subjects and variations in oscillation frequencies across individuals (Fig. S2).

In this procedure, first we used Morlet wavelets (wave number 6) to compute the power of the neuronal oscillations throughout the task at 129 frequencies logarithmically spaced from 2 to 32 Hz. To identify narrowband oscillations at each site, we fit a line to each patient's mean power spectrum in log–log coordinates using a robust linear regression (Fig. S1;[20,21,60]). We then subtracted the actual power spectrum from the regression line. This normalized power spectrum provides a "whitened" version of the signal that removes the $1/f$ background signal and emphasizes narrowband oscillations as positive deflections. We identified narrowband peaks in the normalized power spectrum as any local maximum greater than one standard deviation above the mean[20].

Next, we implemented a spatial clustering algorithm to identify oscillation clusters—contiguous groups of electrodes in each subject that exhibited narrowband oscillations at the same frequency. First, considering a series of 2-Hz-wide intervals centered at 2 to 32 Hz in 1-Hz steps, we identified all the electrodes that exhibited a narrow-band oscillatory peak within that range. We counted the number of electrodes with oscillatory peaks at each frequency, and computed local maxima as potential oscillation clusters. We then tested whether the electrodes that contributed to each local maximum comprised a spatially contiguous group. We found all the electrodes with a peak in the 2-Hz interval around each local maximum and created a pairwise-adjacency matrix to judge their spatial proximity. This matrix indicated whether each electrode pair was separated by less than 15 Talairach units (15 mm). Finally, we used this adjacency matrix to identify mutually connected spatial clusters of electrodes by computing the connected components of this graph using Tarjan's algorithm[61]. We included in our subsequent analyses only the clusters with four or more electrodes.

Importantly, our spatial clustering algorithm adapts to the specific spatial orientation of each patient's ECoG electrode organization by utilizing the electrode's Talairach coordinates rather than the labeled positions from the clinical recordings. Thus, our methods are capable of identifying oscillation clusters that span multiple ECoG grids or strips (e.g., Fig. 1H), rather than being limited to identifying signals within regularly structured electrode arrays[12,13,20].

Identifying traveling waves. Having identified groups of electrodes with oscillations at the same frequency, we next sought to identify traveling waves. Intuitively, a traveling wave can be described as an oscillation that moves progressively across a region of cortex. Quantitatively, a traveling wave can be described as a set of simultaneously recorded neural oscillations at the same frequency whose instantaneous phases vary systematically with the location of the recording electrode. Although many types of traveling waves are possible[14,52], we focused our analyses here on one specific form of this phenomenon, the planar wave[12]. A planar wave would appear in our dataset as an oscillation cluster whose instantaneous phases exhibited a linear relationship with electrode location.

We followed the following procedure to identify planar waves in the phases from each oscillation cluster. First, we measured the instantaneous phases of the signals across each oscillation cluster by applying a Butterworth filter to the signals from each electrode at the cluster's narrowband peak frequency (3-Hz bandwidth). Then we perform the Hilbert transform on each electrode's filtered signal to extract the instantaneous phase at each timepoint[62]. To facilitate visualization, we rotate the phase distributions so that the smallest value is set to 0.

We used circular statistics to identify planar waves of phase progression across each oscillation cluster[27]. For each spatial phase distribution, we used a two-dimensional circular–linear regression to assess whether the observed phase pattern varied linearly with the electrode's coordinates in 2-D. In this regression, for electrode i, x_i and y_i represent the 2-D coordinates and θ_i is the instantaneous phase. x and y are determined by projecting the 3-D Talairach coordinates for each cluster into the best-fitting 2-D plane. Circular–linear models do not have an analytical solution and must be fitted iteratively[27]. A 2-D circular–linear model has three parameters to be fit: the phase slopes a and b, which each correspond to the rate of phase change (or spatial frequencies) in each dimension, and the phase offset θ.

We converted this model to polar coordinates to simplify fitting. This polar model has two parameters: The angle of wave propagation α, defined as $\alpha = \text{atan2}(b, a)$, and the spatial frequency ξ, defined as $\xi = \sqrt{a^2 + b^2}$. We fit α and ξ to the distribution of oscillation phases at each timepoint by conducting a grid search over $\alpha \in [0°, 360°]$ and $\xi \in [0, 18]$ in increments of 5°and 0.5°/mm, respectively. (Note that $\xi = 18$ corresponds to the spatial Nyquist frequency of 18°/mm.)

The model parameters for each timepoint are fitted to produce a phase distribution that most closely matches the phases observed across the electrode cluster. For each value of α and ξ, we compute the estimated phase $\hat{\theta}_i$ at each electrode i as

$$\hat{\theta}_i = (ax_i + by_i + \vartheta) \bmod 360°,$$

where $a = \xi \cos(\alpha)$ and $b = \xi \sin(\alpha)$. Then we compute the goodness of fit for these parameters, which is calculated as the mean vector length $\bar{r}$ of the residuals between the estimated ($\hat{\theta}_i$) and actual (θ_i) phases,

$$\bar{r} = \sqrt{\left[\frac{1}{n}\sum_{i=1}^{n}\cos(\theta_i - \hat{\theta}_i)\right]^2 + \left[\frac{1}{n}\sum_{i=1}^{n}\sin(\theta_i - \hat{\theta}_i)\right]^2},$$

which is the standard approach for evaluating circular–linear models[27]. The selected values of α and ξ are chosen to maximize $\bar{r}$.

Figure S3 illustrates the results of performing this procedure for several trials from Patient 1. The fitted model coefficients indicate physical characteristics of any identified planar traveling wave, by showing the slope and direction of the spatial phase gradient: α is the wave's instantaneous propagation direction and ξ is spatial frequency (i.e., rate of phase change over space) in °/mm.

To measure the statistical reliability of each fitted traveling wave we examined the phase variance that was explained by the best fitting model. As in earlier work[63], we adapted the r^2 goodness-of-fit measure from linear correlation for use with circular data. To do this, we computed the circular correlation ρ_{cc} between the predicted ($\hat{\theta}$) and actual (θ) phases at each electrode[63]:

$$\rho_{cc} = \frac{\sum_{i=1}^{n}\sin(\theta_i - \bar{\theta})\sin(\hat{\theta}_i - \bar{\hat{\theta}})}{\sqrt{\sum_{i=1}^{n}\sin^2(\theta_i - \bar{\theta})\sum_{i=1}^{n}\sin^2(\hat{\theta}_i - \bar{\hat{\theta}})}},$$

where bar denote averaging across electrodes. We squared the result to compute ρ_{cc}^2. Finally, we applied an adjustment to account for the number of fitted model parameters:

$$\rho_{adj}^2 = 1 - \frac{(1-\rho_{cc}^2)(n-1)}{n-k-1}.$$

where n is the number of electrodes, and k is number of independent regressors (k=3). We refer to ρ_{adj}^2 as *phase gradient directionality* (PGD) in the main text, similar to Ref.[13].

Classification of traveling waves. The procedure described above identifies the phase gradients in a single phase distribution. Next, we describe the procedure we used to measure the reliability of each phase gradient in terms of its PGD and directional consistency. First, we computed the PGD for each trial and cluster from its mean spatial phase distribution. We computed the median PGD for each cluster (across trials) and compared this value with the distribution of PGDs estimated from a shuffling procedure (1,000 iterations). In this shuffling procedure, on each trial we compute a single PGD value after randomly permuting the locations of individual electrodes within each cluster, while preserving all other features of the data. We identify reliable traveling waves as electrode clusters in which the actual PGD value exceeds 95% of the distribution of PGD values from shuffling. Due to the spatial permuting that occurs in the shuffling, this method ensures that the traveling waves we identify more reliably exhibit consistently propagating planar waves compared to other types of phase patterns with less structure[64].

Finally, here we considered only the electrode clusters with traveling waves that propagated in a consistent direction over time. To do this, after identifying the clusters with reliable PGD values, we computed for each cluster the distribution of propagation directions (α) across trials. The clusters we designate as exhibiting significant traveling waves are the ones that exhibit a non-uniform distribution of propagation directions, as determined by the Rayleigh test[27] at $p < 0.05$. We calculated the directional consistency (DC) of each cluster as the circular mean vector length of this distribution of propagation directions. Thus, a cluster with DC=1 indicates that its traveling waves always propagate in an identical direction.

Statistical assessment of traveling-wave properties. We performed a series of analyses to compare the properties of traveling waves between clusters from different brain regions. To compare directional propagation between different traveling waves, we first converted each cluster's mean propagation direction into Talairach coordinates. Note that this sometimes caused directional plots to appear distorted, when the 2-D plane for each cluster was skewed relative to the Talairach axes (e.g., Fig. 1). Then, to assess regional differences in propagation directions (Fig. 2B), we grouped each cluster according to whether it was in the frontal, temporal or occipitoparietal region. When a cluster's electrodes were present in multiple areas, we labeled it to the lobe that contained the majority of its electrodes.

To measure the temporal frequency f of a traveling wave, we followed $f = d\bar{\theta}/dt$, where $\bar{\theta}$ is the average phase at each timepoint, taken as the circular mean across electrodes, and t is time. We used this approach to assess each wave's propagation speed v as $v = f/\xi$, where f is instantaneous temporal frequency and ξ is the spatial frequency. Using this equation we calculated each traveling wave's speed at each timepoint. To summarize the propagation speed for each wave (Fig. 5C & S6A), we computed the median propagation speed across all timepoints, excluding periods where the model fit was poor (i.e., mean PGD < 0.5;[13]). We then computed the average propagation speed for each cluster by computing the mean speed across all the timepoints where mean PGD ≥ 0.5. Twenty one clusters had no timepoints with mean PGD ≥ 0.5 and thus were excluded from this analysis.

To assess the role of traveling waves in behavior, for each cluster we compared the properties of traveling waves between trials where the patient had fast or slow responses to the probe in the memory task (median split). Then, for each cluster we computed the mean values of several properties of traveling waves separately for fast and slow trials: power, temporal frequency, PGD, spatial frequency, and directional consistency (Tab. S3). To identify task-related changes in wave DC, we computed the trend of DC over the course of each trial (Fig. 4B). DC slope trend is computed as the Pearson correlation between mean DC and time in each trial. Unless otherwise specified, we used Student's t-tests and ANOVAs to compare differences between regions, with rejection of the null hypothesis reported after FDR correction[65] at $q = 0.05$.

Model of traveling waves based on weakly coupled oscillators. A linear array of weakly coupled Kuramoto oscillators[35] produces traveling waves when it exhibits two properties: (1) weak phase coupling only between neighboring oscillators and (2) a spatial frequency gradient. In this spatial frequency gradient, the intrinsic frequency of each oscillator systematically varies with position along the array[14,36]. This configuration explains the appearance of traveling waves in the digestive system[66] and is hypothesized to generate traveling waves in the cortex[14].

We simulated this model to demonstrate that the frequency gradient we observed in our data (Fig. 6A) is feasible for producing traveling waves that propagate in the directions we observed (Fig. 1). As in earlier work[14], we implemented the Kuramoto model as

$$\frac{d\theta_i}{dt} = \omega_i + \epsilon[\sin(\theta_{i-1} - \theta_i) + \sin(\theta_{i+1} - \theta_i)].$$

where i indexes separate oscillators, ω_i is an oscillator's intrinsic frequency, θ_i is the instantaneous phase, and ϵ is the strength of phase coupling between neighboring oscillators. We used this model to simulate ten oscillators, which vary in frequency from 2 Hz to 16 Hz ($\omega_i = 1.56i + 0.44$ for $i \in [1, 10]$), corresponding to a decreasing posterior-to-anterior frequency gradient from oscillator 10 to 1. Our simulations showed that when there is no cortico-cortico coupling ($\epsilon = 0$), each oscillator exhibits independent oscillations (Fig. 6E)—this resembles the spatial frequency gradients we observed in individual subjects (Fig. S5) and at the population level (Fig. 5D). When coupling is positive ($\epsilon \gg 0$), the same distribution of intrinsic frequencies produces a traveling wave propagating in a posterior-to-anterior direction (Fig. 6F–G).

Acknowledgements

J.J. acknowledges support from NIH Grant MH104606. We wish to thank Jonathan Miller, Salman Qasim, and Melina Tsitsiklis for technical discussions, and Michael Kahana for help with data collection. Raw data for this paper are available at `http://memory.psych.upenn.edu/`. The authors have no competing financial interests.

References

[1] Bragin, A. *et al.* Gamma (40-100 Hz) oscillation in the hippocampus of the behaving rat. *Journal of Neuroscience* **15**, 47–60 (1995).

[2] Jacobs, J., Kahana, M. J., Ekstrom, A. D. & Fried, I. Brain oscillations control timing of single-neuron activity in humans. *Journal of Neuroscience* **27**, 3839–3844 (2007).

[3] Fries, P. A mechanism for cognitive dynamics: neuronal communication through neuronal coherence. *Trends Cogn Sci* **9**, 474–480 (2005).

[4] Kopell, N. J., Gritton, H. J., Whittington, M. A. & Kramer, M. A. Beyond the connectome: the dynome. *Neuron* **83**, 1319–1328 (2014).

[5] Buzsáki, G. & Draguhn, A. Neuronal oscillations in cortical networks. *Science* **304**, 1926–1929 (2004).

[6] Raghavachari, S. *et al.* Theta oscillations in human cortex during a working memory task: Evidence for local generators. *Journal of Neurophysiology* **95**, 1630–1638 (2006).

[7] Watrous, A. J., Tandon, N., Conner, C. R., Pieters, T. & Ekstrom, A. D. Frequency-specific network connectivity increases underlie accurate spatiotemporal memory retrieval. *Nature Neuroscience* **16**, 349–356 (2013).

[8] Freeman, W. & Schneider, W. Changes in spatial patterns of rabbit olfactory EEG with conditioning to odors. *Psychophysiology* **19**, 44–56 (1982).

[9] Freeman, W. J., Rogers, L. J., Holmes, M. D. & Silbergeld, D. L. Spatial spectral analysis of human electrocorticograms including the alpha and gamma bands. *Journal of neuroscience methods* **95**, 111–121 (2000).

[10] Agarwal, G. *et al.* Spatially distributed local fields in the hippocampus encode rat position. *Science* **344**, 626–630 (2014).

[11] Zanos, T. P., Mineault, P. J., Nasiotis, K. T., Guitton, D. & Pack, C. C. A sensorimotor role for traveling waves in primate visual cortex. *Neuron* **85**, 615–627 (2015).

[12] Lubenov, E. V. & Siapas, A. G. Hippocampal theta oscillations are travelling waves. *Nature* **459**, 534–539 (2009).

[13] Rubino, D., Robbins, K. A. & Hatsopoulos, N. G. Propagating waves mediate information transfer in the motor cortex. *Nature Neuroscience* **9**, 1549–1557 (2006).

[14] Ermentrout, G. & Kleinfeld, D. Traveling Electrical Waves in Cortex Insights from Phase Dynamics and Speculation on a Computational Role. *Neuron* **29**, 33–44 (2001).

[15] Bullock, T. *et al.* Eeg coherence has structure in the millimeter domain: subdural and hippocampal recordings from epileptic patients. *Electroencephalography and clinical neurophysiology* **95**, 161–177 (1995).

[16] Menon, V. *et al.* Spatio-temporal correlations in human gamma band electrocorticograms. *Electroencephalography and Clinical Neurophysiology* **98**, 89–102 (1996).

[17] Sternberg, S. High-speed scanning in human memory. *Science* **153**, 652–654 (1966).

[18] Raghavachari, S. *et al.* Gating of human theta oscillations by a working memory task. *Journal of Neuroscience* **21**, 3175–3183 (2001).

[19] Jacobs, J. & Kahana, M. J. Neural representations of individual stimuli in humans revealed by gamma-band electrocorticographic activity. *Journal of Neuroscience* **29**, 10203–10214 (2009).

[20] Zhang, H. & Jacobs, J. Traveling theta waves in the human hippocampus. *The Journal of Neuroscience* **35**, 12477–12487 (2015).

[21] Manning, J. R., Jacobs, J., Fried, I. & Kahana, M. J. Broadband shifts in local field potential power spectra are correlated with single-neuron spiking in humans. *Journal of Neuroscience* **29**, 13613–13620 (2009).

[22] Moran, P. Notes on continuous stochastic phenomena. *Biometrika* 17–23 (1950).

[23] Prechtl, J., Cohen, L., Pesaran, B., Mitra, P. & Kleinfeld, D. Visual stimuli induce waves of electrical activity in turtle cortex. *Proceedings of the National Academy of Sciences* **94**, 7621–7626 (1997).

[24] Patel, J., Fujisawa, S., Berényi, A., Royer, S. & Buzsáki, G. Traveling theta waves along the entire septotemporal axis of the hippocampus. *Neuron* **75**, 410–417 (2012).

[25] Patten, T. M., Rennie, C. J., Robinson, P. A. & Gong, P. Human cortical traveling waves: dynamical properties and correlations with responses. *PloS ONE* **7**, e38392 (2012).

[26] Bahramisharif, A. *et al.* Propagating neocortical gamma bursts are coordinated by traveling alpha waves. *The Journal of Neuroscience* **33**, 18849–18854 (2013).

[27] Fisher, N. I. *Statistical Analysis of Circular Data* (Cambridge University Press, Cambridge, England, 1993).

[28] Klimesch, W. EEG alpha and theta oscillations reflect cognitive and memory performance: a review and analysis. *Brain Research Reviews* **29**, 169–195 (1999).

[29] Voytek, B. *et al.* Shifts in gamma phase–amplitude coupling frequency from theta to alpha over posterior cortex during visual tasks. *Frontiers in Human Neuroscience* **4** (2010).

[30] Groppe, D. M. *et al.* Dominant frequencies of resting human brain activity as measured by the electrocorticogram. *NeuroImage* **79**, 223–233 (2013).

[31] Massimini, M., Huber, R., Ferrarelli, F., Hill, S. & Tononi, G. The sleep slow oscillation as a traveling wave. *The Journal of Neuroscience* **24**, 6862–6870 (2004).

[32] Takahashi, K., Saleh, M., Penn, R. D. & Hatsopoulos, N. G. Propagating waves in human motor cortex. *Frontiers in human neuroscience* **5** (2011).

[33] Jensen, O. & Tesche, C. D. Frontal theta activity in humans increases with memory load in a working memory task. *European Journal of Neuroscience* **15**, 1395–1399 (2002).

[34] Onton, J., Delorme, A. & Makeig, S. Frontal midline EEG dynamics during working memory. *NeuroImage* **27**, 341–356 (2005).

[35] Kuramoto, Y. Rhythms and turbulence in populations of chemical oscillators. *Physica A: Statistical and Theoretical Physics* **106**, 128–143 (1981).

[36] Ermentrout, G. & Kopell, N. Frequency plateaus in a chain of weakly coupled oscillators, i. *SIAM Journal on Mathematical Analysis* **15**, 215–237 (1984).

[37] Giocomo, L., Zilli, E., Fransen, E. & Hasselmo, M. Temporal Frequency of Subthreshold Oscillations Scales with Entorhinal Grid Cell Field Spacing. *Science* **315**, 1719 (2007).

[38] O'Keefe, J. & Recce, M. L. Phase relationship between hippocampal place units and the EEG theta rhythm. *Hippocampus* **3**, 317–30 (1993).

[39] Huerta, P. T. & Lisman, J. E. Bidirectional synaptic plasticity induced by a single burst during cholinergic theta oscillation in CA1 in vitro. *Neuron* **15**, 1053–1063 (1995).

[40] Hyman, J. M., Hasselmo, M. E. & Seamans, J. K. What is the functional relevance of prefrontal cortex entrainment to hippocampal theta rhythms? *Frontiers in Neuroscience* **5**, 24 (2011).

[41] Liebe, S., Hoerzer, G. M., Logothetis, N. K. & Rainer, G. Theta coupling between v4 and prefrontal cortex predicts visual short-term memory performance. *Nature Neuroscience* **15**, 456–462 (2012).

[42] Canolty, R. T. *et al.* High gamma power is phase-locked to theta oscillations in human neocortex. *Science* **313**, 1626–1628 (2006).

[43] VanRullen, R. & Koch, C. Is perception discrete or continuous? *Trends in Cognitive Sciences* **7**, 207–213 (2003).

[44] Freeman, W. The Wave Packet: An Action Potential for the 21st Century. *Journal of Integrative Neuroscience* **2**, 3–30 (2003).

[45] Jezek, K., Henriksen, E. J., Treves, A., Moser, E. I. & Moser, M.-B. Theta-paced flickering between place-cell maps in the hippocampus. *Nature* **478**, 246–249 (2011).

[46] Van Essen, D., Anderson, C. & Felleman, D. Information processing in the primate visual system: an integrated systems perspective. *Science* **255**, 419–423 (1992).

[47] Badre, D. & D'Esposito, M. Is the rostro-caudal axis of the frontal lobe hierarchical? *Nature Reviews Neuroscience* **10**, 659 (2009).

[48] Harry, B. B., Umla-Runge, K., Lawrence, A. D., Graham, K. S. & Downing, P. E. Evidence for integrated visual face and body representations in the anterior temporal lobes. *Journal of cognitive neuroscience* (2016).

[49] Bastos, A. M. *et al.* Visual areas exert feedforward and feedback influences through distinct frequency channels. *Neuron* **85**, 390–401 (2015).

[50] Alexander, D. M. *et al.* Traveling waves and trial averaging: The nature of single-trial and averaged brain responses in large-scale cortical signals. *Neuroimage* **73**, 95–112 (2013).

[51] Freeman, W. J. & Barrie, J. M. Analysis of spatial patterns of phase in neocortical gamma eegs in rabbit. *Journal of neurophysiology* **84**, 1266–1278 (2000).

[52] Muller, L. *et al.* Rotating waves during human sleep spindles organize global patterns of activity that repeat precisely through the night. *eLife* **5**, e17267 (2016).

[53] Viventi, J. *et al.* Flexible, foldable, actively multiplexed, high-density electrode array for mapping brain activity in vivo. *Nature neuroscience* **14**, 1599–1605 (2011).

[54] Khodagholy, D. *et al.* Neurogrid: recording action potentials from the surface of the brain. *Nature neuroscience* **18**, 310–315 (2015).

[55] Liou, J.-y. *et al.* Multivariate regression methods for estimating velocity of ictal discharges from human microelectrode recordings. *Journal of Neural Engineering* **14**, 044001 (2017).

[56] Jacobs, J., Hwang, G., Curran, T. & Kahana, M. J. EEG oscillations and recognition memory: Theta correlates of memory retrieval and decision making. *NeuroImage* **15**, 978–87 (2006).

[57] Michel, C. M. *et al.* EEG source imaging. *Clinical Neurophysiology* **115**, 2195–2222 (2004).

[58] Ezzyat, Y. *et al.* Direct brain stimulation modulates encoding states and memory performance in humans. *Current Biology* **27**, 1–8 (2017).

[59] Talairach, J. & Tournoux, P. *Co-planar stereotaxic atlas of the human brain* (Verlag, Stuttgart, 1988).

[60] Lega, B., Jacobs, J. & Kahana, M. Human hippocampal theta oscillations and the formation of episodic memories. *Hippocampus* **22**, 748–761 (2012).

[61] Tarjan, R. Depth-first search and linear graph algorithms. *SIAM Journal on Computing* **1**, 146–160 (1972).

[62] Freeman, W. Hilbert transform for brain waves. *Scholarpedia* **2**, 1338 (2007).

[63] Kempter, R., Leibold, C., Buzsáki, G., Diba, K. & Schmidt, R. Quantifying circular–linear associations: Hippocampal phase precession. *Journal of Neuroscience Methods* **207**, 113–124 (2012).

[64] Maris, E., Fries, P. & van Ede, F. Diverse phase relations among neuronal rhythms and their potential function. *Trends in Neurosciences* **39**, 86–99 (2016).

[65] Genovese, C. R., Lazar, N. A. & Nichols, T. E. Thresholding of statistical maps in functional neuroimaging using the false discovery rate. *NeuroImage* **15**, 870–878 (2002).

[66] Diamant, N. E. & Bortoff, A. Nature of the intestinal low-wave frequency gradient. *American Journal of Physiology–Legacy Content* **216**, 301–307 (1969).